

An Investigation into Empirical Ice Density Formulations for Dry Ice Growth on Cylinders

Pavlo Sokolov^{1,†}, Muhammad S. Virk¹

¹ Institute of Industrial Technology, University of Tromsø – The Arctic University of Norway, Post Box 385, 8505, Narvik

†Corresponding Author Email: pavlo.sokolov@uit.no

ABSTRACT

This paper describes an investigation into the empirical accreted icing density formulations, namely the numerical fits by (Makkonen and Stallabrass, 1984) and (Jones, 1990). Typically, the icing severity is estimated by the masses of the accreted ice, however, for this study the focus is primarily on the accreted ice densities and thicknesses for the main purpose of estimating the ice loads, in particular for the cases when the ice mass measurements are not readily available and other indirect measurements such as observed ice thicknesses can be used as an estimate. The results were obtained for both the analytical and numerical modeling in comparison with the icing tunnel experiments. Seven different diameters of cylinders ranging from 20 to 298 mm are used. Analysis show that Makkonen and Stallabrass (M&S) fit tends to have good agreement with the smaller cylinders, while it tends to underestimate the icing thicknesses for the larger cylinder diameters. On the other hand, the Jones ice density formulation shows consistently better results for almost all tested cases and especially for the larger cylinder diameters. The results with the MVD approximation show good agreement mainly for smaller diameter cylinders whereas the agreement for the larger cylinders is not good primarily due to low values of droplet inertia parameter K , which puts the results using the MVD approximation outside of the verified range of the current icing theory. Thus, calculations with the full droplet distribution spectrum are recommended.

Keywords: Ice accretion; Ice density; Ice thickness; Cylinder; Droplet distribution spectrum; MVD.

1. INTRODUCTION

The interest in modeling ice accretion on cylindrical objects primarily comes from preventing structural damage or collapse of objects such as overhead transmission lines or communication masts due to the accreted ice mass leading to dynamical instabilities. The theoretical modelling of icing is covered by ISO 12494, where the icing theory framework is valid for the droplet overall collision efficiency range of $0.07 < E < 0.63$ (Makkonen *et al.*, 2018), though, the ISO 12494 model framework scope is rather limited when it comes to the long term modeling of the in-cloud icing events on the power lines and structures. Such long-term icing events can lead to significant ice loads over longer timeframes, where the ice can accrete in multiple “stages” under different operating conditions. These events can be more critical in remote areas, where frequent monitoring of structures and accreted ice is unlikely.

The primary attribute of continued ice accretion, which is the change of the object’s characteristic length, in case of circular structures this length being the diameter, have been theoretically modeled by (Makkonen, 1984). However, the accreted ice mass and its density govern the change in the object’s diameter. While the accreted ice mass and its modeling is the primary focus of the ISO 12494 theoretical framework, the accreted ice density had received less attention in it. This may be critical if direct measurements of the accreted ice deposit on the structure cannot be performed and only indirect measurements such as visual estimation of deposit thickness can be performed.

Currently, there are several empirical accreted ice density formulations, such as (Macklin, 1962), (Pfaum and Pruppacher, 1979), (Bain and Gayet, 1983), (Makkonen and Stallabrass, 1984), (Jones 1990) etc. As noted in (Jones, 1990) all empirical ice density formulations, which are based on the usage of the Macklin parameter, were obtained based on the cold room icing wind tunnel experimental results (Macklin, 1962), (Makkonen and Stallabrass, 1984), instrumented wind tunnel in natural conditions (Bain and Gayet, 1983), or in cloud chamber (Pfaum and Pruppacher, 1979). On the contrary, the empirical ice density in (Jones, 1990) was developed based on the multicylinder measurements in natural conditions on Mt. Washington.

These empirical ice density formulations are also incorporated in the modern CFD solvers, which have now become increasingly popular for the modeling of atmospheric icing on structures. Therefore, the focus of this study is to ascertain how these empirical icing density formulations, both in the analytical and numerical analyses are suitable for modeling of ice density and thickness, in order to investigate their suitability for modeling of long-term icing events, especially when the direct ice masses measurements are not available.

55 **2. MODELS SETUP**

2.1. Analytical Model

The cloud impingement parameters are calculated in accordance to (Finstad *et al.*, 1988):

60
$$X(K, \phi) = [C_{X,1} K^{C_{X,2}} \exp(C_{X,3} K^{C_{X,4}}) + C_{X,5}] - [C_{X,6} (\phi - 100)^{C_{X,7}}] \times [C_{X,8} K^{C_{X,9}} \exp(C_{X,10} K^{C_{X,11}}) + C_{X,12}] \quad (1)$$

where X is either the overall collision efficiency E , the stagnation line collision efficiency β_0 , the maximum impingement angle α_{max} , or the non-dimensional impact velocity V_0 . The values of constants $C_{X,n}$ can be found in (Finstad *et al.*, 1988).

The spectrum-averaged cloud impingement parameters are calculated as:

65
$$X(K, \phi)_{spec} = \sum w_i X(K_i, \phi) \quad (2)$$

where K is the droplet inertia parameter, and ϕ is the Langmuir parameter, defined as (Langmuir and Blodgett, 1946):

70
$$K_i = \frac{\rho_a d_i^2 v}{9 \mu_a D} \quad (3)$$

$$\phi = \frac{18 \rho_a^2 D v}{\rho_d \mu_a} = \frac{Re^2}{K} \quad (4)$$

75 where ρ_a and ρ_d are air and droplet's densities, respectively, μ_a is the density of air, D is the cylinder diameter, v is the operating wind speed and Re is the droplet's Reynolds number. Moreover, w is the volume fraction, d_i is the droplet MVD with the subscript "i" referring to the i th bin of the droplet distribution spectrum and subscript "spec" referring to the spectrum-averaged values. In the analytical model the constraint $X_i(K_i, \phi) = 0.01$ for $K_i \leq 0.17$ is used as per (Finstad *et al.*, 1988).

80 The ice deposit diameter D_i of cylinder is calculated as (Makkonen, 1984):

$$D_i = \left[\frac{4(M_i - M_{i-1})}{\pi \rho_i} + D_{i-1}^2 \right]^{1/2} \quad (5)$$

85 where M is the mass accretion value per unit length, ρ is the ice density and subscript i indicates the time step. In all analytical calculations the time step used is $t = 15$ seconds. This is to ensure that the cylinder rotates at least 360° degrees along its longitudinal axis on each time step to ensure even ice deposit on the cylinder surface, in accordance with (Makkonen, 1984). The accreted ice density at any given time step is calculated as (Makkonen and Stallabrass, 1984):

90
$$\rho_i = 378 + 425 \log_{10}(R) - 82.3 (\log_{10}(R))^2 \quad (6)$$

where, R is the Macklin ice density parameter, given as:

95
$$R = -\frac{V_0 d}{2 T_s} \quad (7)$$

where d is the MVD in microns, V_0 is the impact velocity of the droplet in m/s and T_s is the surface temperature of the ice deposit in Celsius. In the case of dry growth the surface temperature of the ice deposit can be obtained numerically as (Makkonen, 1984):

100
$$\frac{2}{\pi} E v w (L_f + c_w t_a - c_i t_s) = h \left[(t_s - t_a) + \frac{k L_s}{c_p p_a} (e_s - e_a) - \frac{r v^2}{2 c_p} \right] + \sigma a (t_s - t_a) \quad (8)$$

105 where L_f and L_s are latent heats of fusion and sublimation respectively, c_w , c_i and c_p are specific heats of water, ice and air respectively, p_a , e_s and e_a are air pressure, saturation water vapor pressures at surface and air temperatures respectively, h is the overall heat transfer coefficient, $k = 0.62$, r is the recovery factor with value of 0.79 being used for cylinder, t_s and t_a are surface and air temperatures in Celsius, σ is the Stefan-Boltzmann constant and $\alpha = 8.1 \times 10^7 \text{ K}^3$. More details on the terms of heat transfer and derivation of heat transfer equations are given in (Makkonen, 1984).

The "intermediate version" of icing density formulation of (Jones, 1990) is given as:

$$\begin{aligned}
110 \quad & \rho = 0.210R^{0.53} & R \leq 10 \\
& \rho = R/(1.15R + 2.94) & 10 < R < 60 \\
115 \quad & \rho = 0.84 & R \geq 60
\end{aligned}$$

115 This parametric fit using the Macklin parameter was obtained using the best-fit curves for three out of six cylinders from the multicylinder device and the observational data from the Mt. Washington. The reason this particular fit is called “intermediate version” is, as noted in (Jones, 1990) it explains less than 50% variation of the observed rime ice densities on the Mt. Washington. Therefore, (Jones, 1990) developed different empirical icing density formulation, using a range of mathematical and statistical arguments, as well as, employing the Buckingham π theorem, statistical and multi-regression analysis. This “final version” of the Jones icing density formulation explains 80% of rime ice density variation on the Mt. Washington and is as (Jones, 1990):

$$125 \quad \rho = 0.249 - 0.0840 \ln \pi_C - 0.00624(\ln \pi_\phi)^2 + 0.135 \ln \pi_K + 0.0185 \ln \pi_K \ln \pi_\phi - 0.0339(\ln \pi_K)^2 \quad (9)$$

where π_K is the droplet inertia coefficient, π_ϕ is the Langmuir parameter and the term π_C is the ratio of the convective heat flux and the heat flux due to droplet freezing and is defined as:

$$130 \quad \pi_C = \frac{k_a(-2T)/D}{wvL_f} \quad (10)$$

130 As noted in (Jones, 1990) when compared to the original empirical icing density formulation in (Macklin, 1962), the Jones ice density formulation should yield higher density values at lower values of the Macklin parameter R and lower ice density values at high values of R . The (Makkonen and Stallabrass, 1984) and (Jones, 1990) empirical icing density formulations will be used in this study to test the performance of these ice density formulations obtained from rather different operating conditions. The choice of these two particular icing density formulations is governed by the fact that they are implemented in their original form in the numerical model, which is detailed in the following subsection.

2.2. Numerical Model

140 The multiphase Computational Fluid Dynamics (CFD) based numerical simulations are carried out using ANSYS FENSAP-ICE, which uses Eulerian water droplet impingement solver. The general Eulerian two-phase model for viscous flow consists of the Navier-Stokes equations augmented by the droplets continuity and momentum equations (FENSAP-ICE User Manual):

$$145 \quad \frac{\partial \alpha}{\partial t} + \vec{\nabla} \cdot (\alpha \vec{V}_d) = 0 \quad (11)$$

$$150 \quad \frac{\partial(\alpha \vec{V}_d)}{\partial t} + \vec{\nabla}[\alpha \vec{V}_d \otimes \vec{V}_d] = \frac{C_D Re_d}{24K} \alpha (\vec{V}_a - \vec{V}_d) + \alpha \left(1 - \frac{\rho_a}{\rho_d}\right) \frac{1}{Fr^2} \quad (12)$$

where the variables α and $V_{d,a}$ are mean field values of, respectively, the water volume fraction and droplet velocity. The first term on the right-hand-side of the momentum equation represents the drag acting on droplets of mean diameter d . It is proportional to the relative droplet velocity, its drag coefficient C_D and the droplets Reynolds number:

$$155 \quad Re_d = \frac{\rho_a d V_{a,\infty} \|\vec{V}_a - \vec{V}_d\|}{\mu_a} \quad (13)$$

and an inertia parameter:

$$160 \quad K = \frac{\rho_d d^2 V_{a,\infty}}{18 L_\infty \mu_a} \quad (14)$$

where L_∞ is the characteristic length of the object. In case of the cylinder, the characteristic length is cylinder radius as opposed to diameter in analytical model. However, the use of a constant 18 in denominator ensures that inertia parameters are equal in analytical and numerical models. The second term represents buoyancy and gravity forces and is proportional to the local Froude number:

$$165 \quad Fr = \frac{\|\vec{V}_{a,\infty}\|}{\sqrt{L_\infty g_\infty}} \quad (15)$$

170 These governing equations describe the same physical droplets phenomenon as Lagrangian particle tracking approach. Only the mathematical form in which these equations are derived changes using Partial Differential Equations instead of Ordinary Differential Equations. The droplet drag coefficient is based on an empirical correlation for flow around spherical droplets, or:

$$C_D = (24/Re_d) (1 + 0.15Re_d^{0.687}) \quad \text{for } Re_d \leq 1300$$

175

$$C_D = 0.4 \quad \text{for } Re_d > 1300$$

The local and overall collision efficiencies are calculated following a completely different approach, when compared to Finstad et al. The local and overall collision efficiencies are calculated as follows:

$$\beta = -\frac{\alpha V_d \vec{n}}{w V_\infty} \quad (16)$$

180

where α is the local volume fraction (kg/m^3) and \vec{n} is the surface normal vector. The overall collision efficiency is an integration of local collision efficiencies over surface area and is given as:

$$\beta_{tot} = \frac{\int \beta dA}{L_\infty^2} \quad (17)$$

185

The turbulence model used in this study is Menster's SST $k-\omega$ model (FENSAP-ICE User Manual), (Wilcox, 1988). For surface roughness NASA sand-grain roughness model is used which is computed with an empirical NASA correlation for icing (FENSAP-ICE User Manual), (Shin and Bond, 1992).

190 Finally, the icing density formulations used in the numerical model are (Makkonen and Stallabrass, 1984) (referred in FENSAP-ICE as “*Macklin*”) and both intermediate (referred in FENSAP-ICE as “*Jones (glaze)*”) and the actual final rime ice density formulation (Jones, 1990), (referred in FENSAP-ICE as “*Jones (rime)*”), with their mathematical formulations being identical to formulations given in previous section. In order to avoid the potential confusion with the naming of different icing density parameterizations, the “M&S” will be used to refer to Makkonen and Stallabrass fit and “*Jones (glaze)*” and “*Jones (rime)*” will be used to refer to the intermediate and final versions, respectively, of the Jones icing density formulations. This naming convention will be used from this point throughout the rest of manuscript.

195

2.3. Experimental Setup

200 The icing wind tunnel experiments were conducted at Cranfield University icing wind tunnel facility. This is a “closed-loop” tunnel with 761 x 761 mm test section and is capable of operating wind speeds of Mach 0.1 to Mach 0.5, with wide range of possible droplet sizes and Liquid Water Content (LWC) due to flexible spray bars configuration. The operating parameters used for this study are summarized in Table 1.

Table 1. Operating conditions.

Parameter	Value
Cylinder diameter (mm)	20, 50.05, 80.25, 99, 149.5, 249, 298
Air velocity (m/s)	30
Air temp. (°C)	-25
Altitude (m.a.g.l)	0
MVD (μm)	16.36
Liquid Water Content (g/m^3)	0.6
Icing duration (min)	20 (for 20 – 80 mm), 30 (for 99 – 298 mm diameter cylinders)
Cylinder length (mm)	50.04, 50, 67.85, 69.5, 83.5, 111.74, 50, 50

205 The choice of the operating air temperature is based on the need to maintain the “dry growth” regime during experimentation so that the sticking and accretion efficiencies, $\alpha_2 = \alpha_3 = 1$, respectively. The choice of LWC and MVD is based on the need to obtain a measurable ice thickness, while simultaneously keeping the droplet inertia parameter K low. The choice of wind speed corresponds to the minimum rated wind speed for the Cranfield University icing wind tunnel. During the experiments, the rotating multicylinder device, mounted in the center of the test section, was used. The rotational velocity during the experiments was set to 4 RPM. Two cylinder configurations were tested – the configuration consisting of smaller cylinders 20 – 80.25 mm in diameter, and a configuration, consisting of larger cylinders, 99 – 298 mm in diameter. The reason for testing two different configurations is that the used multicylinder device can only allow mounting of four cylinders at a time.

210

215 The choice of only rotating cylinder is based on several considerations, primarily:

1. To keep the results strictly within ISO 12494 modeling framework.

2. According to the experiments of (Makkonen and Stallabrass, 1984) on wires, the rate of rotation was in between 65 and 223 deg/hr, with large jumps in rotation occurring. This implies that for longer time period of at least several hours of ice accretion the resultant ice shape will be circular.
- 220 3. Moreover, (Makkonen, 1984) referencing Howe and Dranevic states that the ratio of the minor to the major axis on actual power line conductors is 0.88 for glaze and 0.82 for rime, on the average.
4. Following personal discussions with Bjørn Eigil Nygård (Kjeller Vindteknikk AS, Norway) and, Egill Thorsteins (EFLA Iceland), it was noted that all significant ice accretions on test spans are circular in nature.
- 225 To minimize the effect of blockage, the multicylinder device was mounted as close as possible to the center of the tunnel's test-section. The duration of the tests was chosen to give a measurable thickness of the ice deposit. Since the large cylinder configuration has significantly lower values of droplet inertia parameter and by extension – the overall collision efficiency, the test duration was increased to 30 min for large configuration in order to offset this. During the experiments the cylinders were video recorded from multiple angles, in order to
- 230 observe the ice growth in the details. Examples of final ice shapes from the experiments is given in Fig. 1.



Fig. 1. Final ice shapes of the small (left) and large (right) cylinder configurations.

- 235 Figure 2 shows intermediate ice shapes for the larger cylinder configuration during the experimentation with 10 min increments and the final ice shapes for the individual cylinders.

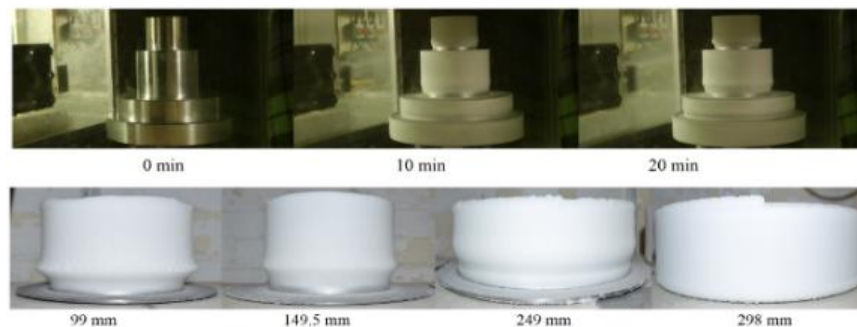


Fig. 2. Intermediate and final ice shapes for the large cylinder configuration. The respective diameters of each cylinders are indicated.

- 240
- The droplet distribution spectrum from the icing wind tunnel is given in Fig. 3. The MVD of this distribution is 16.36 μm . The droplet distribution spectrum was measured using laser diffraction methods, while (Makkonen and Stallabrass, 1984) measured their experimental droplet distribution spectra using Forward Scattering Spectrometer Probe (FSSP) in addition to the common oiled and soothed slides methods, and (Jones, 1990) estimates LWC, MVD and droplet distribution spectra based on the numerical fitting of accreted ice on the multicylinder device at Mt. Washington observatory. In order to check the stability of the operating conditions during icing wind tunnel experiments the water and air pressure in the spray bar configuration was monitored constantly. The subsequent analysis of the water and air pressure fluctuations showed that these fluctuations
- 245
- 250 are within 1% of the specified operating values.

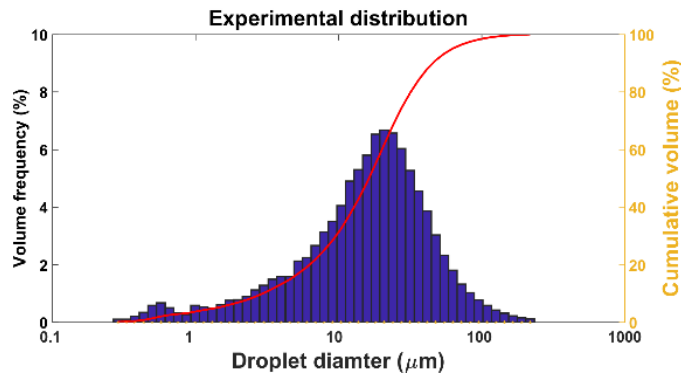


Fig. 3. Droplet distribution spectrum for the Cranfield University (CU) experimental cases.

255 3. RESULTS AND DISCUSSION

3.1. Analytical Analysis

260 Table 2 shows the values of the droplet inertia parameter, end iced cylinder diameter, denoted D_{end} and the accreted ice density, respectively. The analytical results in Table 2 are given as spectrum-averaged mean values taken as average from all time steps and are calculated with the full droplet distribution spectrum from Fig. 3. The experimentally measured values of the end iced cylinder diameters are given as a reference in the “Exp.” column.

Table 2. Values of droplet inertia parameter, end cylinder diameter and accreted ice density in analytical calculations with full droplet distribution spectrum.

D (mm)	K			D_{end} (mm)				ρ (kg/m ³)		
	M&S	Jones (glaze)	Jones (rime)	M&S	Jones (glaze)	Jones (rime)	<i>Exp.</i>	M&S	Jones (glaze)	Jones (rime)
20	9.623	9.188	10.069	29.70	32.39	27.34	32.30	636.9	495.8	856.0
50.05	4.317	4.316	4.499	57.37	60.37	55.72	60.45	590.6	416.2	770.8
80.25	2.871	2.821	2.890	86.25	89.28	85.10	87.57	554.5	366.2	690.3
99	2.328	2.280	2.342	107.08	111.55	105.74	113.72	534.3	341.3	645.2
149.5	1.586	1.566	1.590	156.02	160.27	160.30	155.36	488.5	293.7	545.9
249	0.989	0.982	0.988	253.87	257.60	257.58	254.06	415.1	234.4	399.6
298	0.840	0.836	0.839	302.38	305.83	302.91	307.06	384.3	214.2	342.9

265 In general, the analytical values of end iced diameter calculated with the Jones (glaze) ice density formulation yields the closest agreement with the experimental values in most test cases. Comparatively, the M&S and the Jones (rime) icing density formulations tends to underestimate the ice thicknesses for majority of cylinders with exceptions being 149.5 and 249 mm cylinders, for which the M&S numerical fit gives the closest agreement with the experimental values. In addition, the Jones (glaze) icing density formulation has the lowest overall values of accreted ice densities, as evidenced from Table 2, with Jones (rime) Jones icing density formulation having highest values of accreted ice densities up to 249 mm cylinder, where the M&S formulation shows the best agreement with experimental values.

275 When it comes to the spectrum-averaged results, the biggest difference will be in the values of the droplet inertia parameter K , when compared to the results with the MVD approximation. This increase in the value of K will lead to the increase of the droplet impact velocities, as follows from the structure of Eq. (1), which will, correspondingly, increase the values of the Macklin parameter R . As noted in (Jones, 1990), the numerical fit of (Makkonen and Stallabrass, 1987) produces higher values of ice density than the original formulation by (Macklin, 1962). On the other hand, the Jones (glaze) formulation predicts higher densities for low values of R and lower densities for high values of R than were obtained by (Macklin, 1962).

280 This property of the spectrum-averaging can also explain why the Jones (rime) formulation tends to predict highest densities for almost all cases, with exception of two largest cylinder of 249 and 298 mm diameters. Instead of relying on the Macklin parameter, this formulation relies directly on the values of K and ϕ . While ϕ is independent of droplet diameter, the values of K will increase dramatically when one foregoes MVD approximation for calculations with full droplet distribution spectrum, especially, with the distribution as “wide” as experimental distribution in Fig. 3.

285 On the subject of the MVD approximation, Table 3 shows the analytical results of the droplet inertia parameter, end cylinder diameters and ice densities, respectively, in analytical calculations using MVD approximation as per ISO 12494 modeling framework. The primary interest in producing these values using the MVD

290 approximation is to examine how the spectrum-averaged values compare to those, obtained by strict adherence with ISO 12494 modeling guidelines.

Table 3. Values of droplet inertia parameter, end cylinder diameter and accreted ice density in analytical calculations with the MVD approximation.

D (mm)	K			D_{end} (mm)				ρ (kg/m ³)		
	M&S	Jones (glaze)	Jones (rime)	M&S	Jones (glaze)	Jones (rime)	<i>Exp.</i>	M&S	Jones (glaze)	Jones (rime)
20	2.239	2.174	2.257	29.72	32.10	30.07	32.30	649.0	521.1	641.1
50.05	1.042	1.028	1.038	56.09	58.83	57.82	60.45	575.2	394.5	451.6
80.25	0.672	0.669	0.670	84.34	86.91	86.85	87.57	502.3	308.3	313.9
99	0.545	0.542	0.540	103.92	107.41	108.39	113.72	455.8	265.9	241.0
149.5	0.366	0.367	0.362	152.6	155.07	159.36	155.36	329.2	184.9	100.0
249	0.221	0.224	0.225	251.06	251.06	251.06	254.06	100.0	100.0	100.0
298	0.185	0.187	0.188	300.06	300.06	300.06	307.06	100.0	100.0	100.0

295 From Table 3 it can be seen that while the ice density and iced cylinder diameters are comparable to those in Table 2 for the smaller cylinder configuration of 20 – 80 mm cylinders as well as the 99 mm cylinder. For the 149.5 mm cylinder, the values of end cylinder diameter, while being lower than the spectrum-averaged values for all formulations, still agrees well with the experimental values.

300 However, the agreement in end cylinder diameter values becomes poor for the two largest cylinders, for which the calculated ice density is below the minimum constraint of 100 kg/m³. This constraint is used in the analytical model as an assumed estimation on the lower bound of the accreted ice density. Moreover, when comparing the values of the droplet inertia parameter in Tables 2 and 3, the significantly lower values of K in Table 3 will result in lower values of the cloud impingement parameters, in particular, when it comes to the droplet impact velocities and Macklin parameter values, thus significantly decreasing the accreted ice density values.

305 This, coupled with the MVD approximation yielding smaller values of end cylinder diameters for majority of cases in Table 6, will primarily result in an underestimation of the accreted ice masses calculated with MVD approximation, when compared to the spectrum-averaged results. This can potentially limit the applicability of using the MVD approximation in modeling of the long-term icing events, in particular when the droplet inertia parameter is low. Finally, for the MVD approximation both versions of the Jones formulation tend to be in good agreement for majority of cases, with obvious exception of two largest cylinders, where both of them are below constraint of 100 kg/m³, unlike with the spectrum-averaged values, where Jones (rime) Jones shows consistently higher densities.

310 This does suggest that the procedure of spectrum-averaging might not be directly admissible for this formulation, due to significantly higher values of K the spectrum-averaging method produces. Contrary, the M&S and Jones (glaze) Jones formulations do not experience such sharp drop in values, as the effect on spectrum-averaging on the droplet impact velocities is not as pronounced as in the case with droplet inertia parameter, with the increase in droplet impact velocities being enough to offset the ice densities going below constraint in the spectrum-averaged values.

3.2. Numerical Analysis

320 Table 4 shows the results from the CFD simulations using the full droplet distribution spectrum from Fig. 3.

Table 4. Values of droplet inertia parameter, end cylinder diameter and accreted ice density in numerical calculations with full droplet distribution spectrum.

D (mm)	K			D_{end} (mm)				ρ (kg/m ³)		
	M&S	Jones (glaze)	Jones (rime)	M&S	Jones (glaze)	Jones (rime)	<i>Exp.</i>	M&S	Jones (glaze)	Jones (rime)
20	4.747	6.683	9.427	79.68	50.80	30.19	32.30	40.7	111.1	473.8
50.05	4.308	4.040	4.349	59.78	67.06	58.74	60.45	376.4	202.3	425.1
80.25	2.799	2.694	2.819	88.80	95.35	87.57	87.57	333.8	181.9	392.9
99	2.320	2.216	2.276	104.92	114.50	108.85	113.72	425.9	233.0	376.7
149.5	1.560	1.525	1.540	153.77	160.77	157.69	155.36	444.6	246.9	343.8
249	0.945	0.936	0.940	251.75	256.37	254.55	254.06	444.7	246.9	295.0
298	0.792	0.786	0.787	299.70	304.36	302.87	307.06	440.5	243.7	276.9

325 In general, the CFD simulations show good agreement with the analytical modeling results for the iced cylinder diameters for 80 – 149.5 mm cylinders. For the 50 mm cylinder, the agreement depends on the formulation used, i.e., M&S and Jones (rime) formulations show better agreement than the Jones (glaze) formulation. For the 20 mm cylinder only Jones (rime) formulation shows good agreement with the rest of formulations producing significantly higher end iced diameters. Moreover, observe that the ice density values in the CFD simulations are consistently lower than in analytical model, with exception of 249 and 298 mm cylinders. The primary reason for it is the difference in the flow treatment between the analytical and the numerical model, as

the analytical model uses the potential flow approximation, as opposed to viscid turbulent flow in the CFD simulations.

In particular, the difference in the accreted ice density between two models simplifies to the difference in the stagnation line impact velocities, which are used in the calculation of the Macklin parameter as given in Eq. (7). Since for majority of cylinders, the analytical and the numerical results tend to have relatively comparable end iced cylinder diameters, this suggests that the CFD simulations produce consistently lower ice accretion masses as well, which may be detrimental, if the long-term extreme value ice modeling is needed. Table 5 shows the CFD simulations results using the MVD approximation. Again, the reason for this is to keep the results consistent with the ISO 12494 framework and to allow direct comparison with the results in Table 3.

Table 5. Values of droplet inertia parameter, end cylinder diameter and accreted ice density in numerical calculations with the MVD approximation.

D (mm)	K			D_{end} (mm)				ρ (kg/m ³)		
	M&S	Jones (glaze)	Jones (rime)	M&S	Jones (glaze)	Jones (rime)	<i>Exp.</i>	M&S	Jones (glaze)	Jones (rime)
20	2.133	1.859	2.226	32.44	40.17	30.25	32.30	374.1	201.1	473.8
50.05	1.054	1.014	1.047	56.11	60.28	56.74	60.45	471.9	270.1	425.1
80.25	0.677	0.662	0.678	84.93	88.76	84.70	87.57	373.4	200.7	392.9
99	0.555	0.548	0.552	102.58	105.06	103.60	113.72	486.4	283.9	376.7
149.5	0.372	0.371	0.371	150.99	152.02	151.65	155.36	494.6	292.2	342.8
249	0.225	0.224	0.224	249.33	249.56	249.53	254.06	481.4	278.9	295.0
298	0.188	0.188	0.188	298.26	298.56	298.45	307.06	473.5	271.5	276.9

The results from Table 5, when compared with the experimental values and the results from Table 3, do produce good agreement for the smaller cylinder configuration, in particular, for the 50 and 80 mm cylinders with Jones (glaze) formulation, and for 20 mm cylinder, using the M&S and the Jones (rime) formulations. However, for the 149.5, 249 and 298 mm cylinders the MVD approximation barely shows any ice accretion, as end iced cylinder diameters are practically unchanged from un-iced diameters.

Furthermore, CFD results with the MVD approximation have somewhat higher values of the accreted ice density than the simulations using the full droplet distribution spectrum, with the exception of Jones (rime) formulation where full droplet distribution spectrum and the MVD approximation values for the ice density are comparable. This difference can be explained by either the difference in surface temperature, differences in the flow regime, primarily due to boundary layer differences, averaging procedures for the full droplet distribution spectrum in the CFD software, or combination of these factors.

Advantageously, the CFD simulations allow for detailed investigation of these details. From the CFD results, the boundary layer is much more pronounced in the simulations using the full droplet distribution spectrum. In addition, the droplet velocity gradients are much more “sharp” for the simulations with full droplet distribution spectrum, while the droplet velocities are higher in the case of simulations with monodisperse distribution. This may explain the higher ice density values in the results using the MVD approximation, and why the results for smaller cylinders in Tables 4 and 5 generally agree for cases with higher K values; as this thicker boundary layer is actively “deflecting” the droplets away from the cylinder. In addition, this can probably explain the considerably higher thicknesses in the analytical results for the 249 and 298 mm cylinders, as the boundary layer is not present in the potential flow approximation, which is used in the analytical results. As an example, Fig. 4 shows the droplet velocity streamlines for a few selected cases in the CFD simulations.

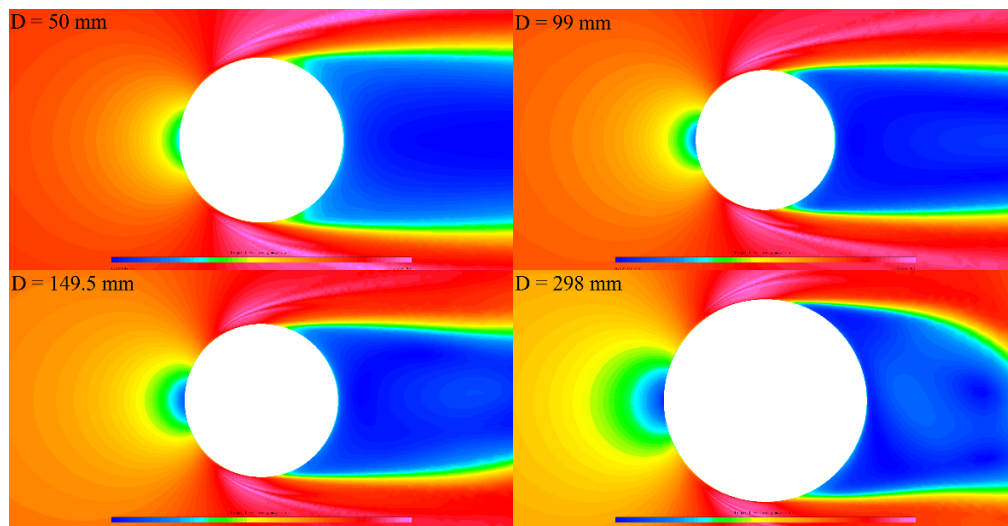


Fig. 4. Droplet velocity contours in the CFD simulations.

370 In Fig. 4, the boundary layer is much more pronounced for the 298 mm and 149 mm cylinders, while for 50
 mm cylinder it is barely visible. This thick boundary layer results in more pronounced flow separation for the
 larger cylinders. Again, this is possible explanation why the CFD simulations with the full droplet distribution
 spectrum tend to underestimate the accreted ice density values, when compared to the analytical and the MVD
 approximation results, as the impact velocities would be lower in this situation, as the thick boundary layer will
 “push out” the droplets from the stagnation region.

375 Based on the comparison of the results between the MVD approximation and full droplet distribution spectrum,
 it can be seen that the MVD approximation works well for higher values of droplet inertia parameter. This
 agrees with statements by (Makkonen *et al.*, 2018) and (ISO, 2001) that the current icing parameterization is
 applicable for the range of the overall collision efficiency of $0.07 < E < 0.63$ and that for $E < 0.1$ the icing
 parameterization using MVD approximation will underestimate the ice accretion, respectively.

380 Thus, in modeling of long-term icing events with expected low values of the droplet inertia parameter and the
 overall collision efficiency, the use of full droplet distribution spectrum is advantageous, as it can reliably
 reproduce accumulated thicknesses in most extreme cases, as evidenced from the results of this study. Still, for
 the more extreme cases, e.g. 249 and 298 mm cylinders, which have very low values of the droplet inertia
 parameter, even full droplet distribution spectrum may underestimate the icing intensity. In those cases, the
 385 recalculation of droplet trajectories using full drag terms is advised (Finstad *et al.*, 1988).

4. VALIDATION

For the validation purposes the experimental cases from the FRonTLINES (Frost and Rime on The Overhead
 Transmission Line) have been selected. These test cases are characterized by the low values of the droplet
 inertia parameter, K , for most of them, except the test cases at 7 m/s wind speeds for which, the K value lies in
 390 “verified range”. The detailed information regarding the operating conditions in these experiments as well as
 the experimental droplet distribution spectrum are given in (Makkonen *et al.*, 2018). Unlike the previous
 experimental cases, discussed previously in this work, in the FRonTLINES cases the end iced masses are
 known, while the end cylinder diameters are unknown. Thus, this combination allows for validation of the
 analytical calculation procedure for the overall collision efficiency and total accreted ice mass. The results of
 395 analytical calculations for the FRonTLINES test cases are given in Tables 6 and 7 for the experimental droplet
 distribution spectrum and the MVD approximation, respectively.

Table 6. Analytical results for FRonTLINES experimental cases with the experimental droplet distribution
 spectrum. The number in brackets shows the wind speed in m/s.

D	D _{end} (mm)	K	ρ (kg/m ³)	M (g)	M _{exp} (g)	E	E _{exp}
M&S							
30 (4)	30.52	0.471	404.3	1.560	1.163	0.115	0.086
50	50.39	0.306	276.8	1.321	0.722	0.058	0.032
80	80.40	0.229	140.0	1.112	0.743	0.031	0.021
100 (4)	100.41	0.209	100.0	1.020	0.770	0.023	0.017
170	170.23	0.181	100.0	0.973	0.812	0.013	0.011
30 (7)	31.07	0.796	574.0	4.600	4.211	0.194	0.177
100 (7)	100.43	0.280	336.2	3.549	4.754	0.045	0.060
Jones (glaze)							
30(4)	30.92	0.469	226.2	1.556	1.163	0.115	0.086
50	50.67	0.305	158.9	1.320	0.722	0.058	0.032
80	80.50	0.229	112.7	1.112	0.743	0.031	0.021
100(4)	100.41	0.209	100.0	1.020	0.770	0.023	0.017
170	170.23	0.181	100.0	0.973	0.812	0.013	0.011
30(7)	31.56	0.790	391.5	4.600	4.211	0.194	0.177
100(7)	100.77	0.280	186.5	3.546	4.754	0.045	0.060
Jones (rime)							
30(4)	30.62	0.471	338.8	1.559	1.163	0.115	0.086
50	50.50	0.305	213.6	1.321	0.722	0.058	0.032
80	80.49	0.229	116.0	1.112	0.743	0.031	0.021
100 (4)	100.41	0.209	100.0	1.020	0.770	0.023	0.017
170	170.23	0.181	100.0	0.973	0.812	0.013	0.011
30 (7)	31.27	0.793	483.3	4.600	4.211	0.194	0.177
100 (7)	100.84	0.280	170.8	3.546	4.754	0.045	0.060

400 Table 7. Analytical results for FRonTLINES experimental cases with the MVD approximation. The number
 in brackets shows the wind speed in m/s.

D	D _{end} (mm)	K	ρ (kg/m ³)	M (g)	M _{exp} (g)	E	E _{exp}
M&S							

30 (4)	30.34	0.302	305.1	0.767	1.163	0.057	0.086
50	50.18	0.182	100.0	0.226	0.722	0.010	0.032
80	80.18	0.170	100.0	0.362	0.743	0.010	0.021
100 (4)	100.18	0.170	100.0	0.453	0.770	0.010	0.017
170	170.18	0.170	100.0	0.769	0.812	0.010	0.011
30 (7)	30.86	0.524	550.1	3.555	4.211	0.150	0.177
100 (7)	100.32	0.170	100.0	0.793	4.754	0.010	0.060
Jones (glaze)							
30 (4)	30.60	0.300	171.0	0.762	1.163	0.056	0.086
50	50.18	0.182	100.0	0.226	0.722	0.010	0.032
80	80.18	0.170	100.0	0.362	0.743	0.010	0.021
100 (4)	100.18	0.170	100.0	0.453	0.770	0.010	0.017
170	170.18	0.170	100.0	0.769	0.812	0.010	0.011
30 (7)	31.31	0.520	359.6	3.542	4.211	0.149	0.177
100 (7)	100.32	0.170	100.0	0.793	4.754	0.010	0.060
Jones (rime)							
30 (4)	30.49	0.301	209.9	0.764	1.163	0.056	0.086
50	50.18	0.182	100.0	0.226	0.722	0.010	0.032
80	80.18	0.170	100.0	0.362	0.743	0.010	0.021
100 (4)	100.18	0.170	100.0	0.453	0.770	0.010	0.017
170	170.18	0.170	100.0	0.769	0.812	0.010	0.011
30 (7)	31.27	0.520	372.8	3.544	4.211	0.149	0.177
100 (7)	100.32	0.170	100.0	0.793	4.754	0.010	0.060

In Tables 6 and 7, the end cylinder diameter in all cases changes insignificantly with maximum diameter increase being barely over 1 mm. This primarily can be explained by the low values of K and the choice of operating conditions, namely, the LWC being equal to 0.4 g/m^3 with the test duration of 30 min. for all cases. Moreover, the results in Table 7 show that the value of K is low enough that for majority of cases the constraint of $E = 0.01$ if $K \leq 0.17$ (Finstad *et al.*, 1988) is enforced. Thus, the analytical results with the MVD approximation tend to underestimate the ice masses and the overall collision efficiencies in most of these cases. On the other hand, the results with experimental droplet distribution spectrum show slightly elevated values of these parameters in the analytical calculations. This may be explained by the nature of spectrum-averaging procedure, as while the smallest bins in the distribution will be bounded by the constraint of $E = 0.01$ if $K \leq 0.17$, for larger bins, for which $K > 0.17$, the collision efficiency value will be calculated “as normal”. As a result, the overall collision efficiency values may be slightly overestimated, when compared to the experimental results, as evidenced in Table 6.

When it comes to the values of the accreted ice densities in Tables 6 and 7, for the majority of cases the calculated accreted ice densities are below the constraint of 100 kg/m^3 , in particular, for the results with the MVD approximation, where all cases, with the exception of 30 mm cylinder are below this constraint. The situation is a bit different for the spectrum-averaged results, where only two largest cylinders are below the constraint. For the cases where the calculated ice density is not below 100 kg/m^3 , a large spread of values can be observed in Tables 6 and 7, with majority of those lying in the range of $250\text{--}400 \text{ kg/m}^3$. This coupled with very low calculated end cylinder diameters suggests that in reality the uniform layer of ice will not form and instead large, individual beads of rime ice will be present, as its expected that the individual bead height will be bigger than $0.5\text{--}1 \text{ mm}$, which is typical difference in the end and start diameter values in Tables 6 and 7.

Thus, for additional validation, different experimental test cases were selected, with higher values of the droplet inertia parameter, namely, two cases from the experiments of (Makkonen and Stallabrass, 1984) – test cases 6 and 16. This particular choice was governed by several reasons, in particular the closeness of diameter values to the ISO 12494 “reference collector” (case 6) and the current “limit value” of verified cylinder diameter validity range (case 16). Moreover, the LWC and MVD values for these two cases are the highest when compared to other experimental cases with same cylinder diameters, thus giving the highest possible accreted ice mass and thickness, compared to other experimental cases. The detailed operating conditions for these test cases is available in (Makkonen and Stallabrass, 1987) Table 1.

As noted in Table 1 in (Makkonen and Stallabrass, 1987) for the analytical calculations one of the three experimental droplet distribution spectra has been used, denoted as “*Droplet size distribution category*”, however, due to significant passage of time the exact information on these droplet distributions is no longer available (Makkonen, personal communication). Thus, for the purpose of the modeling in this paper, these two test cases have been analyzed using the monodisperse distribution, as per ISO 12494 guidelines and the Langmuir D distribution, as it is a common distribution in in-flight icing studies. The results from analytical modeling are given in Table 8.

Table 8. Analytical results for two test cases of (Makkonen and Stallabrass, 1987).

Test	Distribution	K	D _{end} (mm)	D _{end} Exp (mm)	ρ (kg/m ³)	ρ _{exp} (kg/m ³)	M (g)	M _{exp} (g)	E	E _{theory}	E _{exp}
M&S											
6	MVD	1.115	36.15	36.50	762.8	746.1	17.533	18.70	0.299	0.30	0.32
6	LangD	1.515	36.23	36.50	760.0	746.1	17.806	18.70	0.303	0.30	0.32
16	MVD	0.491	78.38	79.50	660.4	710.3	18.296	29.6	0.110	0.14	0.18
16	LangD	0.673	78.96	79.50	681.3	710.3	23.732	29.6	0.142	0.14	0.18
Jones (glaze)											
6	MVD	1.113	36.27	36.50	741.5	746.1	17.536	18.70	0.298	0.30	0.32
6	LangD	1.513	36.35	36.50	738.5	746.1	17.814	18.70	0.302	0.30	0.32
16	MVD	0.489	78.86	79.50	545.6	710.3	18.258	29.6	0.109	0.14	0.18
16	LangD	0.672	79.37	79.50	595.9	710.3	23.722	29.6	0.141	0.14	0.18
Jones (rime)											
6	MVD	1.095	37.47	36.50	581.8	746.1	17.563	18.70	0.294	0.30	0.32
6	LangD	1.500	36.94	36.50	654.7	746.1	17.851	18.70	0.301	0.30	0.32
16	MVD	0.484	80.49	79.50	339.8	710.3	18.130	29.6	0.107	0.14	0.18
16	LangD	0.667	80.53	79.50	437.8	710.3	23.694	29.6	0.140	0.14	0.18

440

In Table 8 the variable “ E_{theory} ” shows the values of the overall collision efficiency as calculated by (Makkonen and Stallabrass, 1987) for comparison purposes to the values of the overall collision efficiency E as calculated in this work. Moreover, the variable “ ρ_{exp} ” shows the experimental value of the accreted ice density, calculated based on the reported ice masses and ultimate cylinder diameters in (Makkonen and Stallabrass, 1987).

445

From Table 8 it can be seen that in analytical calculations, expectedly, the M&S formulation shows the best agreement with experimental results, as this numerical fit was developed based on these experimental results. The Jones (glaze) formulation also shows good agreement for the 31.83 mm cylinder, however, it underestimates the value of accreted ice density for the 76.09 mm cylinder. In terms of accreted ice thicknesses in the analytical results, both Macklin and Jones (glaze) yield good agreement with the experimental values while Jones (rime) parameterization tends to slightly overestimate the ice thicknesses.

450

By summarizing the analytical, numerical and experimental results following conclusions can be made:

- The M&S formulation yields good agreement, in both the analytical and the numerical results for smaller cylinder configuration, 20 – 80 mm in diameter in the Cranfield University experimental cases and the 31.83 and 76.09 mm cylinders from the (Makkonen and Stallabrass, 1984) experimental cases.
- Both versions of the Jones formulation yield better agreement than the M&S formulation for majority of cylinder diameters in the Cranfield University experimental cases.
- The results using the full droplet distribution spectrum yield good agreement with the experimental results, particularly for larger cylinders.
- The results using the MVD approximation only yield acceptable agreement for the smaller cylinder configuration and 31.83 mm cylinder from the (Makkonen and Stallabrass, 1984) experimental cases.
- Between the two Jones formulations, the intermediate (glaze) formulation shows better agreement with experimental values in analytical results with full droplet distribution spectrum and in numerical with the MVD approximation, except 20 mm cylinder, while final (rime) Jones formulation shows opposite results.
- The Jones (glaze) formulation in the Cranfield University cases performed admirably, considering the surface temperature in those conditions is expected to be below -20 °C. This value is a rough “cutoff” as neither (Macklin, 1962) in his experiments nor (Jones, 1990), who employed similar analysis technique to obtain her intermediate version of the icing density parameterization, haven’t tested and/or discarded cases with lower temperature during developing of their respective formulations.
- For the (Makkonen and Stallabrass, 1984) experimental cases, the M&S and the Jones (glaze) parameterizations showed good agreement; however, Jones (rime) formulation was underestimating the ice density. The possible reasons for the underestimation of the experimental ice density by Jones parameterization in the (Makkonen and Stallabrass, 1984) experiments is given in (Jones, 1990).

455

460

465

470

5. CONCLUSION

In this paper the investigation into several empirical accreted ice density formulations have been conducted, with the main goal of assessing how well said empirical formulations can capture the accreted ice thicknesses. The practical purpose of it is to use the accreted ice thickness as a sort of icing severity estimate in modeling of the long-term icing events, if the accreted ice mass is an unknown value. The icing modeling in this study was done by using both the analytical modeling and the CFD simulations, in order to compare two most likely approaches of the modeling of the long term icing events. The obtained icing thicknesses were than compared to experimentally measured values.

475

480

485 The obtained results show that both the analytical and the numerical models can adequately estimate end iced cylinder diameters for majority of the tested cylinder diameters in this study. In particular, while the M&S formulation tends to have good agreement with the smaller cylinder configuration, it tends to underestimate the icing thicknesses for the larger cylinder configuration. On the other hand, the Jones formulations show consistently better results for almost all tested cases, and especially, for the larger cylinder configuration. However, all formulations tend to underestimate the icing thicknesses for the largest cylinders, 249 and 298 mm in diameter.

490 These results were obtained using the full droplet distribution spectrum from the Cranfield University icing wind tunnel. In order to keep the results consistent with the framework of ISO 12494 icing theory, the matching set of values, using the monodisperse droplet distribution with the equal MVD was obtained. The results with the MVD approximation show good agreement mainly for smaller cylinder configuration, 20 – 80 mm in diameter, and the agreement for the larger cylinder diameter is non-satisfactory, primarily due to low values of droplet inertia parameter K for these cases, which puts the results using the MVD outside of the verified range of the current icing theory. Thus, calculations with the full droplet distribution spectrum are recommended. 495 Summarizing the findings of the validation section, both tested formulations based on Macklin parameter, i.e., the numerical fit by Makkonen and Stallabrass and the intermediate version of Jones formulation have showed better agreement than the final version of Jones formulation, however, as noted in the original work (Jones, 1990) there are several reasons for this discrepancy.

ACKNOWLEDGEMENTS

500 The work reported in this paper is funded by the Research Council of Norway, IceBOX – project no. 282403 and WindCoE (*Nordic Wind Energy Centre*) project within the Interreg IVA Botnia-Atlantica, as part of European Territorial Cooperation (ETC). Authors would like to acknowledge Dr. David Hammond, Dr. Hugo Pervier and Mr. Peter West from Cranfield University, UK for assisting during icing tunnel experimentation.

REFERENCES

- 505 1. Bain, M. and Gayet, J. F., (1983). Contribution to the modeling of the ice accretion process. Pp. 13–20 in *Proceedings of the First International Workshop on Atmospheric Icing of Structures*, U. S. Army CRREL Special Report 83–17.
- 510 2. Finstad, K.J., Lozowski, E.P., Gates, E.M., (1988). A computational investigation of water droplet trajectories. *Journal of Atmospheric and Oceanic Technology*, vol. 5, pp. 160-170.
3. *FENSAP-ICE User Manual*
- 515 4. ISO 12494:2001(E), (2001). *Atmospheric icing of structures*. Standard. International Organization for Standardization. Geneva, CH.
5. Jones, K.F. (1990). The density of natural ice accretions related to nondimensional icing parameters, *Quarterly Journal of Royal Meteorological Society*, vol. 116, pp. 477–496.
- 520 6. Langmuir, I., Blodgett, K., (1946). *A Mathematical Investigation of Water Droplet Trajectories*. Army Air Forces technical report 5418. Army Air Forces Headquarters, Air Technical Service Command.
- 525 7. Macklin, W.C., (1962). The density structure of ice formed by accretion. *Quarterly Journal of Royal Meteorological Society*, vol. 88 pp. 30–50.
8. Makkonen, L., (1984). Modeling of Ice Accretion on Wires. *Journal of Applied Meteorology*, vol. 23, pp. 929–939.
- 530 9. Makkonen, L., Stallabrass J.R., (1984). Ice accretion on cylinders and wires. *National Research Council of Canada*. Division of Mechanical Engineering Technical Report TR-LT-05.
10. Makkonen, L., Stallabrass, J.R., (1987). Experiments on the cloud droplet collision efficiency of cylinders. *Journal of Applied Meteorology*, vol. 26, pp. 1406–1411.
- 535 11. Makkonen, L., Zhang, J., Karlsson, T., Tiihonen, M., (2018). Modelling the growth of large rime ice accretions, *Cold Regions Science and technology*, vol. 151, pp. 133–137.
- 540 12. Pfaum, J.C. and Pruppacher, H.R., (1979). A wind tunnel investigation of the growth of graupel initiated from frozen drops. *Journal of Atmospheric Sciences*, vol. 36, pp. 680–689.

13. Shin, J. and Bond, T, (1992). Experimental and Computational Ice Shapes and Resulting Drag Increase for a NACA 0012 Airfoil, *NASA Technical Manual 105743*.
14. Wilcox, D.C., (1988). "Re-assessment of the scale-determining equation for advanced turbulence models", *AIAA Journal*, vol. 26, no. 11, pp. 1299–1310.